



# Moderate Temperature Treatment of Gas-Phase Volatile Organic Toluene Using NiO and NiO–TiO<sub>2</sub> Nano-catalysts: Characterization and Kinetic Behaviors

Fares Almomani<sup>1</sup> · Rahul R. Bhosale<sup>1</sup> · Majeda Khraisheh<sup>1</sup>

Received: 17 June 2020 / Accepted: 30 September 2020 / Published online: 14 October 2020  
© The Author(s) 2020

## Abstract

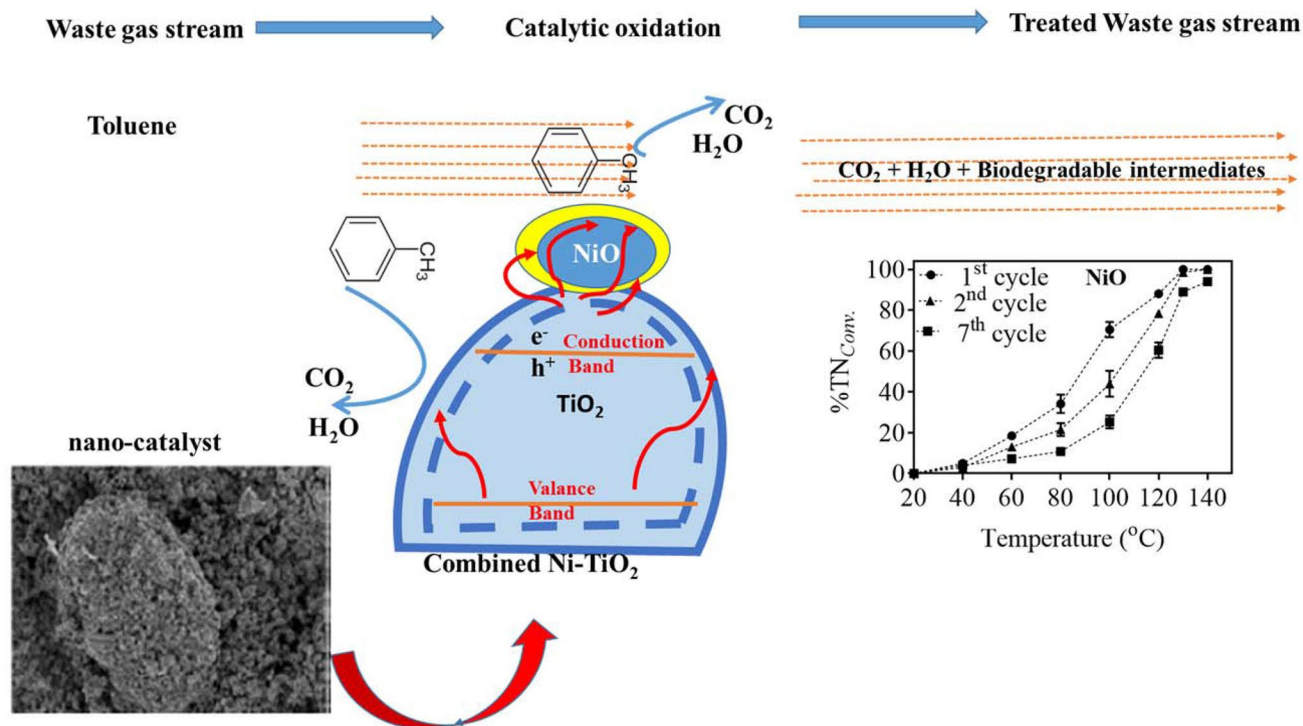
For the first time, the potential of Ni/NiO and NiO–TiO<sub>2</sub> nano-catalysts for the oxidation of toluene under moderate temperatures was investigated. The nano-catalysts were prepared using the solution combustion synthesis method (SCSM) and the effect of the composition of nano-catalysts, the inlet toluene concentration ( $[C_7H_8]_{in}$ ), the relative humidity (RH), and the temperature on the percentage of toluene conversion ( $\%TN_{Conv.}$ ) were subsequently examined. Results revealed that the nano-catalysts synthesized with a low fuel-to-metal ratio produced pure NiO, which has significant catalytic activity toward the conversion of toluene. Conversely, the high fuel-to-metal ratio generated a nano-catalysts that contains a mixture of Ni/NiO or pure Ni with low activity toward the conversion of toluene. Adding NiO to TiO<sub>2</sub> increased the surface area of the catalyst, augmented the catalyst active sites, enhanced the oxidation of toluene, and increased CO<sub>2</sub> selectivity ( $S_{CO_2}$ ). NiO and NiO–TiO<sub>2</sub> nano-catalysts exhibited higher reaction rates, significant catalyst turnover frequency, and low activation energy. The obtained results revealed that the SCSM is a promising synthesis method for producing NiO or NiO–TiO<sub>2</sub> nano-catalysts, which can be employed successfully for the removal of toluene from gas streams.

---

✉ Fares Almomani  
falmomani@qu.edu.qa

<sup>1</sup> Department of Chemical Engineering, College of Engineering, Qatar University, P. O. Box 2713, Doha, Qatar

## Graphic Abstract



**Keywords** CO<sub>2</sub> selectivity · Volatile organic compounds · Degradation products · Industrial contamination

## Statement of Novelty

Industrial emissions of volatile organic compounds (VOCs) can cause substantial air pollution problems and affect human health and the environment. The current study presents for the first time an efficient waste-gas treatment method based on destruction processes rather than the conversion of contaminants from one phase to another. This is the first study that provides an optimization strategy for waste gas treatment under moderate temperature using nano-catalysts in pilot plant configuration. The study also ascertains the treatment mechanism based on the formed radicals and identified by-products.

## Introduction

Volatile organic compounds (VOCs) cause substantial air pollution problems that are harmful to human health and to the environment [1–6]. An increase in environmental awareness has prompted researchers to explore effective treatment technologies to reduce the amount of VOCs in the air [7–10]. Toluene, a common VOC, is an extremely dangerous and

abundant pollutant due to its aromatic structure, which is resistant to conventional treatments and often requires oxidation at low temperatures [11–13]. Additionally, toluene has a long half-life [14] and a photochemical ozone creation potential (POCP) [15, 16]. The presence of toluene has been identified in industrial effluents of printing, paint pressing, and petrochemical industries [11, 17, 18]. Various methods have been implemented to eliminate, and control VOC and toluene emissions [13]. Procedures such as reverse-flow packed bed reactors, bio-filters [19], incineration, distillation, and solid acids have been tested [20–31]. However, the efficiency, durability, and cost of these techniques have made their application difficult.

Among the numerous technologies available for VOCs reduction, catalytic oxidation processes are a more viable option, especially at low concentrations (< 1%) [32–36]. These processes include complete oxidation of the hydrocarbon into water and carbon dioxide, rather than transferring the pollutant from one phase to another. Primarily, the catalytic oxidation of VOCs is carried out using metal oxide [37, 38], noble metals supported on a carbon or inorganic carrier [39–42], or a mixture of metals and their oxides [43–45].

The use of noble metals (e.g. Pt and Pd) have exhibited excellent activity and selectivity for the catalytic oxidation

of VOCs [44, 46]. However, some studies have recommended replacing noble metals with cheaper catalysis due to the high cost [47, 48]. Alternatively, transition metals and their oxides, have displayed a high level of activity, significant selectivity, and resistance against deactivation [49–51]. Barakat et al. [46] and Delannoy et al., [52] demonstrated that the catalytic reactivity of transition metals and their oxides can be enhanced if they are formed as a thin film over inorganic support or as a nano-catalysts with a diameter of < 5 nm. The improvement in catalytic activity was connected to the increase in the surface areas of catalyst, the decrease in the particle size or thickness, and the increase in the number of active sites formed in corners and particle/support interfaces.

The use of NiO nano-catalysts alone or combined with other supports such as thin films have exhibited high catalytic oxidation reactivity toward VOCs [53, 54], and particular interest has been given to the application of NiO-based catalysis. Ni-based catalysts are available, cheap and safe to used. Therefore, have been implemented for hydrogen generation, hydrocarbon, carbon dioxide, and oxygen reforming processes [55–57]. Shaban et al. [58], have used the MCM-48/Ni<sub>2</sub>O<sub>3</sub> composite for the photocatalytic removal of red dye. Recent studies have demonstrated that Ni can be used to catalyze the conversion of CO to CO<sub>2</sub> at lower temperatures in contrast to the high temperatures required by noble metals [59–62]. Other studies have indicated that a thin film of NiO deposited on the support surface possesses a high reactivity and good stability for different processes such as ethanol decomposition, CO, and VOC oxidation [63–66].

The performance of the catalyst toward the oxidation of VOCs depends on the physicochemical properties and morphology of the catalysts, the operating conditions, and the type and composition of the inlet gas stream [67–69]. Esmailirad et al., [70] have suggested that humidity could negatively affect the catalyst activity and the decomposition of the VOCs. Arnold and Sundaresan [71] highlighted a decrease in the oxidation performance of VOCs by increasing the relative humidity (RH) in the feed, which was associated with the competition between water and toluene on the catalyst active site. Within this context, low humidity enhances the VOCs catalytic oxidation because of the formation of OH from the dissociative chemisorption of water vapor [72–74]. However, high humidity increases the chance of water molecule adsorption on the active site of the catalyst which subsequently blocks the adsorption of VOCs, and minimizes the catalytic oxidation efficiency [75, 76].

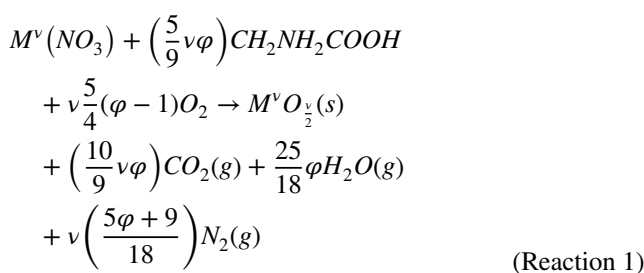
Although various studies have reported the use of Ni and its oxide in the oxidation of hydrocarbons [55, 56, 77], a review of the relevant research literature indicates that only one study reported the use of Ni, NiO, and NiO–TiO<sub>2</sub> for the catalytic oxidation of toluene under low to moderate

temperatures [78]. Therefore, the present work investigated the catalytic activity of pure NiO, a mixture of Ni/NiO, pure Ni, and a film of NiO supported on TiO<sub>2</sub> for the oxidation of toluene under different temperatures. Additionally, the influence of the inlet concentration of toluene ( $[C_7H_8]_{in}$ ), relative humidity (RH), and feed temperature on the conversion performance were investigated. The kinetic parameters, catalyst stability, and the types of oxidation intermediates were examined and discussed. The nano-catalysts were prepared using the SCSM method and characterized using different techniques including Field-Emission scanning electron microscope (SEM), transmission electron microscopy (TEM), Fourier Transform infrared spectroscopy (FTIR), and X-ray diffraction (XRD).

## Materials and Methods

### Preparation of Catalysts

NiO nano-catalysts were synthesized using the SCSM method as it is a widely used approach to synthesize nano-catalysts with the high-surface area. According to this method, the mechanism for nano-catalysts formation is based on the decomposition of glycine and nickel nitrate generating NH<sub>3</sub> and HNO<sub>3</sub> as reaction fuels (RFs). Once generated, the RFs react together in an exothermic reaction creating the required energy to self-sustain high-temperature reaction conditions following Reaction (1) [79, 80]. The stoichiometric equilibrium of the reaction suggests that using high concentration of glycine would create an environment that helped to reduce the formation of metal oxides over pure metals.



where  $M^v$  is the metal valance charge,  $\varphi$  is RF to metal ratio.

Based on Ashok et al. [79], a  $\varphi > 1$  represents a fuel-rich environment, a  $\varphi < 1$  is fuel lean environment, and  $\varphi = 1$  represents stoichiometric conditions where no external oxygen is needed for synthesis.

Different stoichiometric values of nickel nitrate hexahydrate, Ni(NO<sub>3</sub>)<sub>2</sub>·6H<sub>2</sub>O, (Alfa Aesar, 99%) and glycine, CH<sub>2</sub>NH<sub>2</sub>COOH, (Alfa Aesar, 98.5%) were used to synthesis a pure NiO, a mixture of Ni and NiO, and pure Ni, as per

Reaction (1). The  $\text{Ni}(\text{NO}_3)_2 \cdot 6\text{H}_2\text{O}$  and glycine were mixed in a 100 mL of deionized water at 25 °C for 1 h which created a clear homogeneous solution. Then, the mixture was heated using hotplate (Barnstead Thermolyne, model no: sp 46925) under atmospheric pressure and a controlled heating rate of 10 °C/min. when the water evaporated, the temperature of the solution augmented to an ignition point. Thereafter, combustion occurred, which produced gaseous products and the synthesized nano-catalysts. The nano-catalysts were grinded in a hand mortar, sieved < 75  $\mu\text{m}$  sieve, characterized and used in VOC oxidation.

### NiO Supported on $\text{TiO}_2$

The NiO supported on  $\text{TiO}_2$  was prepared by mixing tetrabutyl orthotitanate ( $\text{Ti}(\text{OCH}_2\text{C}_4\text{H}_9)_4$ ) with acetylacetone ( $\text{C}_5\text{H}_8\text{O}$ ), n-propanol ( $\text{C}_3\text{H}_8\text{O}$ ), and deionized water in a volumetric ratio of 1.0:0.5:5.0:0.5 at a controlled temperature of 25 °C. Acetyl acetone acts as a chelating agent which controls the hydrolysis of tetrabutyl orthotitanate. The mixture was blended gently for 30 min. Subsequently, the NiO added to the resulting mixture at a ratio of 1 mL mixture to 0.5 mg NiO under continuous mixing, left to react for another 30 min, dried at 85 °C and annealed at 450 °C for 1 h at atmospheric pressure.

### Characterization of Catalyst

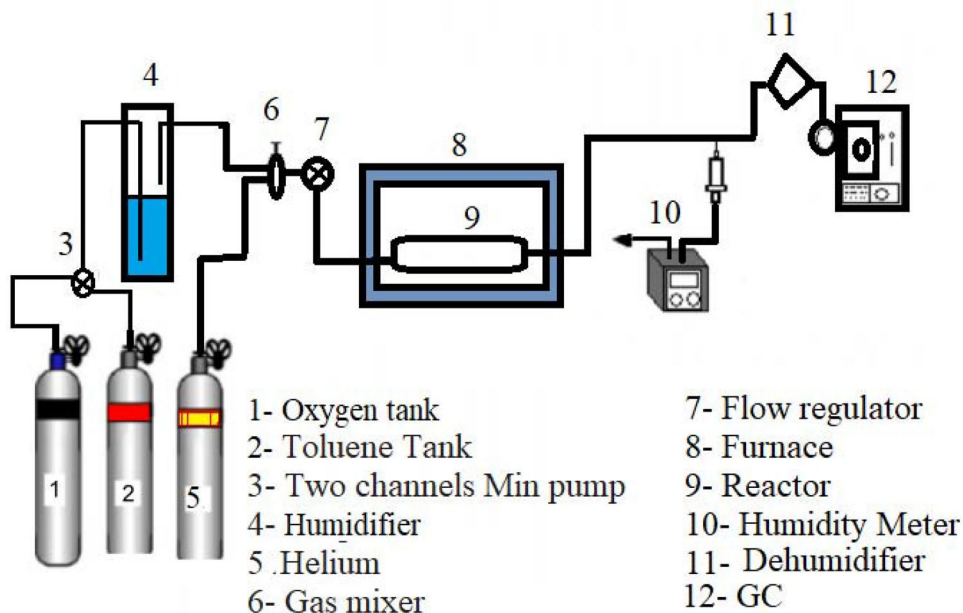
Field-Emission scanning electron microscope (SEM), transmission electron microscopy (TEM), Fourier Transform infrared spectroscopy (FTIR), and X-ray diffraction (XRD) were used to measure the surface area, structure and

morphology of the synthesized nano-catalysts (NiO and  $\text{NiO-TiO}_2$ ). Surface area measurements were carried out in a Quanta-chrome autosorb-1 using nitrogen as adsorbent gas. The nano-catalysts were outgassed at 473 K and the pressure was gradually reduced at rate of 25  $\mu\text{Hg min}^{-1}$  followed by immersion in a liquid nitrogen bath. X-ray diffraction (XRD) measurements were conducted in the air using a Scintag X-ray diffractometer with Cu-K $\alpha$  radiation wavelength of 1.54056 Å. The nano-catalysts microstructures were imaged using a Field-Emission SEM (Magellan 400 (FEI) that provides a nondestructive ultra-high resolution imaging.

### Experimental Set-Up

The catalytic decomposition of toluene was carried out using a flow-type reaction system (Fig. 1). The installation consisted of toluene (Aldrich, purity 99.8%), pure oxygen (Aldrich, purity 99.99%), helium (Aldrich, purity 99.998%) tanks, a humidifier, a gas mixer, a reactor, and a gas chromatograph. The reactor is comprised of a quartz chamber (ID = 25 mm, L = 350 mm) surrounded by a tubular furnace. The outlet of the reaction unit was linked to a humidity meter and a gas chromatograph (GC, Perkin Elmer Clarus 500) for effluent gas analysis. The mass flow rate of the inlet air mixture to the reactor was measured and controlled by a mass flow controller (MFC, MKS Instruments, USA). The temperatures of toluene and the humidifier were controlled at  $25 \pm 2$  °C. The toluene vapor had the  $[\text{C}_7\text{H}_8]_{\text{in}}$  in the range of 10–80 ppm and was constantly supplied into the reactor. The concentrations of influent and effluent streams were measured by the GC, which is equipped with a thermal conductivity detector (TCD). A thermocouple inserted

Fig. 1 Experimental setup



inside the quartz reactor was used to monitor the reaction temperature. The temperature of the furnace was monitored using a controller that was connected to a PC. Heating cycles were conducted at a rate of 3 °C min<sup>-1</sup>.

### Experimental Procedure

The oxidation of toluene over Ni/NiO and NiO–TiO<sub>2</sub> nano-catalysts was conducted at atmospheric pressure in a continuous flow packed reactor. The inlet gas to the reactor was produced by mixing Toluene, C<sub>i</sub>=400 ppmv with water from the humidifier (T=25 °C and p=685 mmHg). The gas was mixed with high purity O<sub>2</sub> and helium. Subsequently, the gas mixture (Toluene, O<sub>2</sub>, He, and water vapor) which had a flow rate in the range of 0.1 to 0.5 L.min<sup>-1</sup> was introduced into the reactor. To adjust the toluene concentration, two O<sub>2</sub> streams were used. The first was introduced into the humidifier to maintain a constant flow rate of toluene vapor. The second balanced the overall concentration. The inlet and outlet stream concentrations were analyzed using an on-line GC (TCD) using several columns (Shin Carbon ST, Q PLOT, 2 OV101, and molecular sieve) to quantify the toluene, O<sub>2</sub>, CO<sub>2</sub>, CO, and Benzene. The detection limit for all of the gases was determined to be in the range of 0.7 ± 0.02 ppmv.

### Mathematical Manipulation

The inlet and outlet concentrations of toluene and the concentration of effluent gases (toluene, O<sub>2</sub>, CO<sub>2</sub>, CO) were utilized to determine the percentage toluene conversion (%TN<sub>Conv.</sub>), as displayed in Eq. (1), the selectivity of catalyst toward CO<sub>2</sub> (S<sub>CO<sub>2</sub></sub>) as displayed in Eq. (2), the reaction rate (r) as shown in Eq. (3), and turnover frequency (TOF) as illustrated in Eq. (4).

$$\%TN_{Conv.} = \frac{[C_7H_8]_{in} - [C_7H_8]_{out}}{[C_7H_8]_{in}} * 100\% \tag{1}$$

$$S_{CO_2}(\%) = \frac{[CO_2]_{outlet} * 100}{7 * [Toluene]_{initial} * \%TN_{conv.}} \tag{2}$$

$$r \left( \text{mole s}^{-1} \text{ g}_{nanocatalyst}^{-1} \right) = \frac{\text{Molar flow rate of toluent} \left( \text{mole s}^{-1} \right) * \%TN_{Conv.}}{\text{mass of nano - powder}(\text{g})} = \frac{Q(\text{L s}^{-1}) * \left[ \frac{1 \text{ mol}}{22.4 \text{ L}} * \frac{273 \text{ K}}{298 \text{ K}} \right] * \%TN_{Conv.}}{\text{mass of nano - powder}(\text{g})} \tag{3}$$

$$TOF \left( \text{s}^{-1} \right) = \frac{r \left( \text{mole s}^{-1} \right)}{\frac{\left( MW_{NiO} \left( \frac{\text{g}}{\text{mole}} \right) * 600 \right)}{\left( \rho \left( \frac{\text{g}}{\text{m}^3} \right) * d(m) * a_{pt} \left( \text{m}^2 \right) * N_A \right)}} \tag{4}$$

where [C<sub>7</sub>H<sub>8</sub>]<sub>in</sub> and [C<sub>7</sub>H<sub>8</sub>]<sub>out</sub> are the initial and final concentrations of toluene, [CO<sub>2</sub>]<sub>outlet</sub> is the concentration of CO<sub>2</sub> in the effluent gas, Q is the gas flow rate (L s<sup>-1</sup>), MW<sub>NiO</sub> is the molecular weight of NiO (g mole<sup>-1</sup>), ρ is the density of NiO (g m<sup>-3</sup>), d is the average particle diameter (m) (from SEM images), a<sub>pt</sub> is the surface area of one NiO atom (m<sup>2</sup>), and NA is Avogadro’s number.

## Results and Discussion

### Characterization of Catalyst

Figure 2a illustrates how the produced nano-catalysts have a spherical shape with tightly agglomerated nanocrystallites porous structure and individual particle size in the range of 10–50 nm. Figure 2b displays the XRD distribution of the final products of nano-catalysts at different fuel/metal ratios of 0.5, 1, and 1.75. The ϕ value has a significant effect on the composition of the nano-catalysts with a general trend showing the change from pure NiO product at ϕ ≤ 0.5 to a mixture of Ni-NiO at 0.5 < ϕ < 1.75 and pure Ni at ϕ ≥ 1.75. Table 1 presents the average, maximum, and minimum crystal sizes of nano-catalysts mixture at ϕ of 0.5, 1, and 1.75 as calculated from the XRD measurement. Results indicated an increase in the crystal size by increasing the ϕ value. The nano-catalysts prepared with ϕ = 0.5 (i.e. pure NiO) has an average crystal size of 428.5 Å, followed by pure Ni (ϕ ≥ 1.75) has an average crystal size of 342.6 Å. Lastly, the mixture of Ni-NiO nano-catalysts prepared with ϕ = 1 demonstrated an average crystal size of 317.0 Å. As the nano-catalysts prepared with ϕ = 0.5 exhibited the highest crystal size, it was thereafter selected to be combined with TiO<sub>2</sub> and used for toluene oxidation. The composition of the Ni-NiO nano-catalysts was determined by the mass balance calculations and revealed that it contains 20 mol% nickel and the balance nickel oxide.

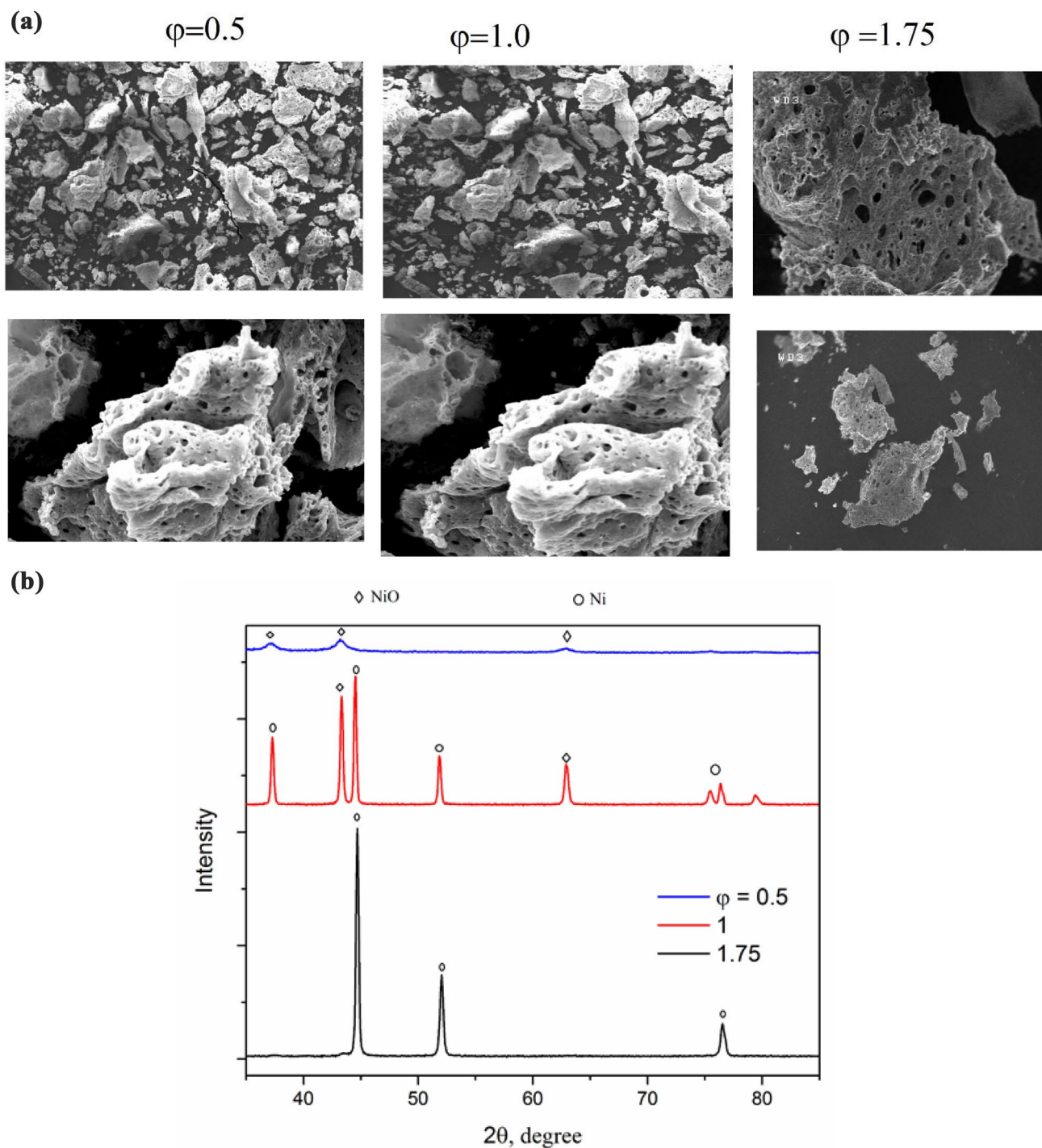


**Fig. 2** a SEM and b XRD images of the Ni–NiO nano-catalysts prepared at different metal to fuel ratios ( $\varphi$ )

Figure 3a–c shows the SEM images, XPS spectra, and XRD patterns of the NiO supported on TiO<sub>2</sub> (i.e. NiO–TiO<sub>2</sub> nano-catalysts). The NiO–TiO<sub>2</sub> has a homogenous structure with an average size of 19.5 nm. A lattice spacings of  $0.22 \pm 0.03$  nm and  $0.25 \pm 0.01$  nm were associated with cubic planes of NiO and TiO<sub>2</sub>, respectively. The XRD test

of the NiO–TiO<sub>2</sub> was compared with NiO (Fig. 3b, c). Pure NiO showed diffraction peaks at 37°, 43°, 63°, 76°, and 79° which is connected to the cubic structure of NiO. NiO–TiO<sub>2</sub> nano-catalyst was observed to have peaks at 24.0°, 36.7°, 43°, 53.9°, 55.1°, which corresponds to the TiO<sub>2</sub> anatase phase. Other peaks observed at 25.1°, 39.2°, 43.6°, and

**Table 1** Average, maximum, and minimum crystal sizes of Ni–NiO nano-catalysts at different fuel to metal ratios ( $\phi$ )

$\phi$	Crystal size (Å)			SD
	Maximum	Minimum	Average	
0.5	854.8	219.3	428.5	8.7
1.0	395.1	254.2	317.0	9.2
1.75	402.25	208.4	342.6	4.5

Calculated from the XRD measurement

57.9° were related to the TiO<sub>2</sub> rutile phase. The high ratio of anatase to rutile suggests the formation of a stabilized anatase phase caused by the annealing processes [81, 82]. The presence of NiO in the structure was combined with a reduction in anatase peaks and the appearance of peaks at 36.2°, 42.1°, 76.1°, and 79.1° which are related to the formation of NiO crystallites. Similar results were reported by

Ahmed et al. [83]. Moreover, the results revealed that Ni<sup>2+</sup> was incorporated within the lattice of TiO<sub>2</sub> by replacing the Ti<sup>4+</sup> ions. The incorporation of Ni<sup>2+</sup> within the lattice of TiO<sub>2</sub> was due to similarity in the ionic radii of Ni<sup>2+</sup> (0.72 Å) as compared with Ti<sup>4+</sup> (0.75 Å) [84].

The discernible trends reflect how nickel ion can be easily introduced into the TiO<sub>2</sub> lattice. Additionally, NiO was likely diffused as amorphous oxide which coated the surface of the anatase phase and prevented changes to the rutile phase. Figure 3d displays the Ni 2p and Ti 2p XPS data of the NiO–TiO<sub>2</sub> nanoparticles. The Ni 2p spectrum highlighted one chemical state of Ni at 854 eV belonging to NiO of the form of Ni 2p<sub>3/2</sub>. No other forms of Ni were observed, which confirms that NiO is the dominant structure [85]. The Ti 2p spectra of NiO–TiO<sub>2</sub> nanoparticles (inner Fig. 3d) was observed to have a peak at approximately 456 eV which corresponds to the binding energy of Ti 2p<sub>3/2</sub> on the form of Ti(IV) state (i.e. TiO<sub>2</sub>).

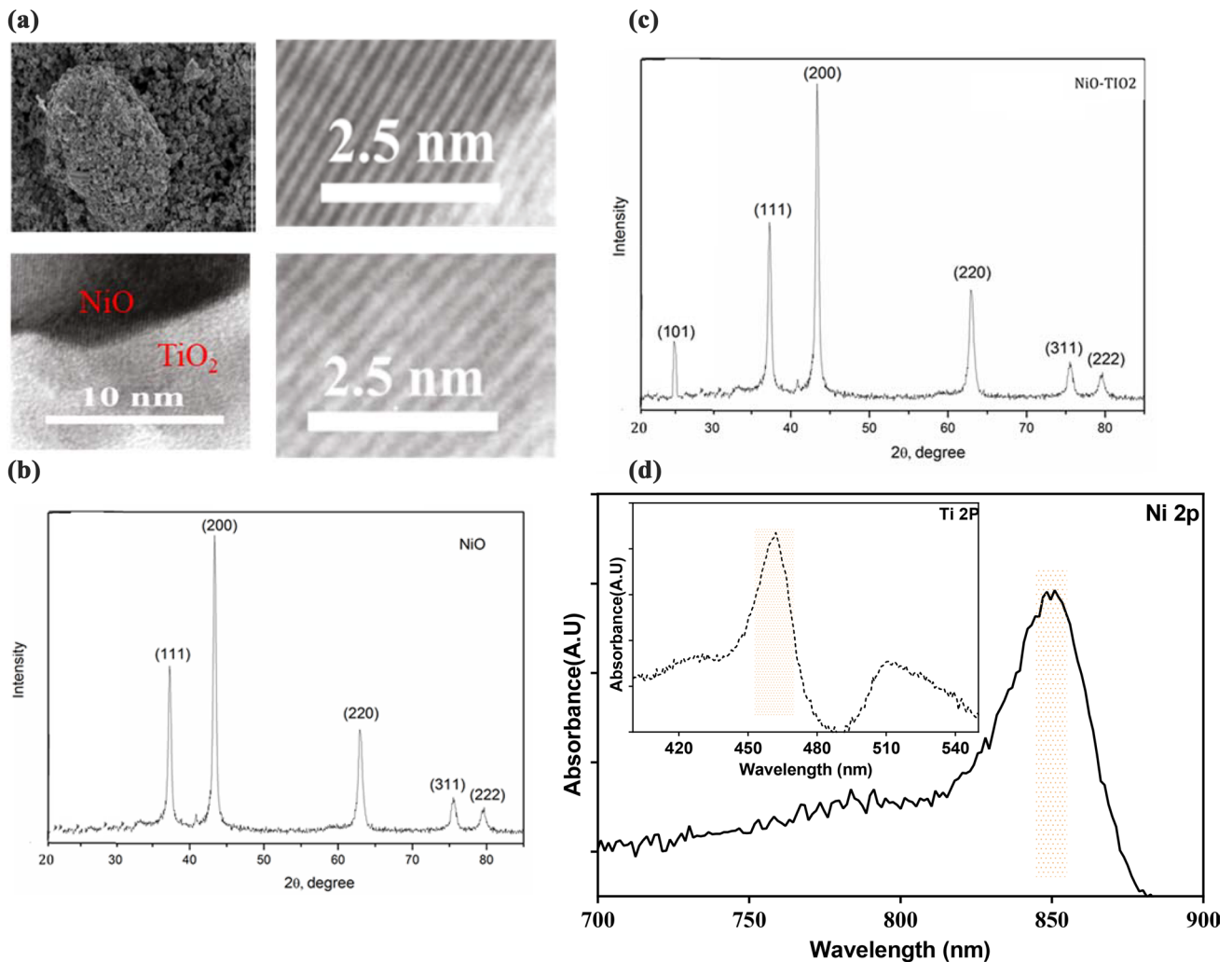


**Fig. 3** a TEM image of NiO–TiO<sub>2</sub> nano-catalysts b XRD patterns of NiO and NiO–TiO<sub>2</sub> nano-catalysts, and c XPS spectra of NiO–TiO<sub>2</sub> nano-catalysts, d external Ni 2p and internal Ti 2p spectra

SEM images were used to calculate the surface area of the nano-catalysts. No less than 10 measurements were carried out for each compound. The results were presented as average values at a 95% confidence interval. NiO was observed to have a surface area of  $135 \pm 5 \text{ m}^2 \text{ g}^{-1}$  (Std. Dev. 4.5) and NiO–TiO<sub>2</sub> had a surface area of  $115 \pm 3 \text{ m}^2 \text{ g}^{-1}$  (Std. Dev. 9.5). The addition of TiO<sub>2</sub> to NiO decreased the surface area, which resulted from its deposition on the surface of TiO<sub>2</sub>.

### Catalytic Oxidation of Toluene

Figure 4 presents the percentage conversion of toluene (%TN<sub>Conv.</sub>) at different cycles (1st, 2nd, and 7th) as a function of temperature over nano-catalysts produced with  $\phi$  of 0.5, 1, 1.75, as well as NiO–TiO<sub>2</sub>. For the tests performed with Ni/NiO there was a distinguishable relationship between the % TN<sub>Conv.</sub> and the composition of nano-catalysts. Pure NiO ( $\phi = 0.5$ ) showed a % TN<sub>Conv.</sub> > 7% at a temperature of 60 °C and proceeded to reach 100% at 123 °C. On the other hand, the nano-catalysts contained a mixture of Ni and NiO required a higher temperature ~ 78 °C to achieve significant % TN<sub>Conv.</sub> of toluene and a temperature  $\geq$  of 158 °C was required to attain % TN<sub>Conv.</sub> of 100%. Alternatively, pure Ni nano-catalysts achieved considerable

% TN<sub>Conv.</sub> of toluene at 75 °C and attained a 100% conversion at 160 °C. The observed trends showed that the composition, physicochemical properties, morphology and structure of the Ni- nano-catalysts play a key role in the conversion of toluene and controlling the operating temperature for maximum removal. The highest conversion was achieved with pure NiO at  $T \leq 65$  °C, in comparison with the nano-catalysts that contain a mixture of Ni–NiO or pure Ni. As previously indicated, pure NiO has large surface areas, which supports greater catalytic activity toward the conversion of toluene. The pure NiO nano-catalysts has larger particle sizes than Ni–NiO or pure Ni that form a weak Ni–O bond on the catalyst surface and contribute to the generation of more reactive oxygen on the surface of the catalyst causing an increase in % TN<sub>Conv.</sub>. Consequently, the degradation of toluene occurs at lower temperatures. The observed trends suggest that the catalytic activity of the Ni-based catalysts can be improved by controlling the synthesis process to produce pure NiO. Tests conducted with NiO–TiO<sub>2</sub> nano-catalysts displayed a substantial improvement in % TN<sub>Conv.</sub> beginning at 40 °C with the majority (100%) of toluene removed at 110 °C. Although the surface area of NiO–TiO<sub>2</sub> ( $115 \pm 3 \text{ m}^2 \text{ g}^{-1}$ ) is lower than NiO ( $135 \pm 5 \text{ m}^2 \text{ g}^{-1}$ ), the significant enhancement in % TN<sub>Conv.</sub> could be caused by the increase in the

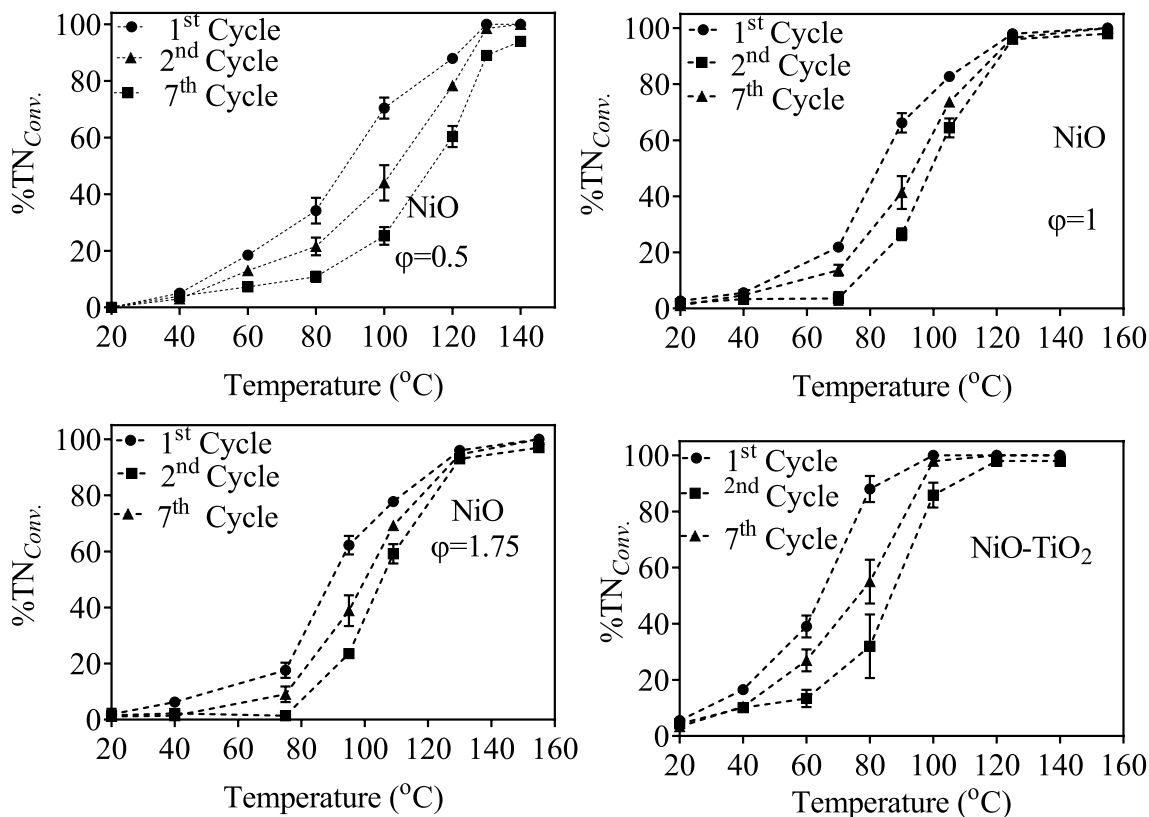


**Fig. 4** % TN<sub>Conv.</sub> as a function temperature over pure NiO ( $\phi = 0.5$ ), pure Ni ( $\phi = 1.75$ ), and mixture of Ni/NiO ( $\phi = 1.75$ ) and NiO–TiO<sub>2</sub> nano-catalysts for 1st, 2nd and 7th cycles. Flow rate =  $0.1 \text{ L min}^{-1}$ , RH = 10%,  $[\text{C}_7\text{H}_8]_{\text{in}} = 40 \text{ ppm}$ , 20% O<sub>2</sub> and the balance He



number of active sites formed in corners and particle/support interfaces. Park et al. [86] demonstrated that NiO and TiO<sub>2</sub> and their combinations have a greater affinity toward toluene oxidation in comparison with other catalysts such as bare-SiO<sub>2</sub>. The performance of all Ni-NiO catalysts are stable over the seven cycles, as the results during these cycles were similar, which indicates that these catalysts have an excellent service life.

The products of toluene conversion were tested using GC-TDC and it was established that under all study conditions, CO<sub>2</sub> was the main product. Benzene and other non-identified hydrocarbons were also detected at % TN<sub>Conv.</sub> ≤ 55. Additionally, no CO was detected in the outlet stream, which confirms the ability of the NiO and NiO–TiO<sub>2</sub> nano-catalysts to catalyze the conversion of toluene to CO<sub>2</sub>. As the % TN<sub>Conv.</sub> increases, the selectivity toward CO<sub>2</sub> ( ) simultaneously increased reaching 100% for % TN<sub>Conv.</sub> of 100. Similar results were reported in studies reported by Rooke et al. [87] and Kim et al. [88]. As the treatment of the toluene, in the present study, was carried out with a synthetic toluene, it is expected that the developed nano-catalysts will still have significant % TN<sub>Conv.</sub> when used with real industrial wastewater. To verify this expectations, a set of experiments were carried

out with gas stream containing a mixture of gases similar to the composition of real industrial VOCs. The preliminary results revealed significant % TN<sub>Conv.</sub>, which is aligned with the results presented in this work. Further testing of real gas streams will be carried out in the future.

**Effect of the Inlet Toluene concentration ([C<sub>7</sub>H<sub>8</sub>]<sub>in</sub>)**

Figure 5 illustrates the effect of the [C<sub>7</sub>H<sub>8</sub>]<sub>in</sub> on the % TN<sub>Conv.</sub>. The results are the average of three repeated experiments at a 95% confidence interval. The experiments were conducted at a gas flow rate of 0.21 L min<sup>-1</sup> with the gas stream consisted of 20% O<sub>2</sub>, the balance He, and relative humidity of 10%. Changing the [C<sub>7</sub>H<sub>8</sub>]<sub>in</sub> showed a minor impact on the reported % TN<sub>Conv.</sub> for a gas-phase reaction carried out at longer Hydraulic retention time (HRT) ≥ 105 s. However, tests conducted at a shorter HRT exhibited a noticeable decrease in the % TN<sub>Conv.</sub> as the [C<sub>7</sub>H<sub>8</sub>]<sub>in</sub> increased. The % TN<sub>Conv.</sub> decreased from 100 to 91% as the HRT decreased from 105 s to of 21 s for the tests carried out with [C<sub>7</sub>H<sub>8</sub>]<sub>in</sub> of 40 ppm. Tests carried out with higher [C<sub>7</sub>H<sub>8</sub>]<sub>in</sub> (e.g. 80 ppm) were observed to have a significant decrease (17%) in the % TN<sub>Conv.</sub> as the HRT decreased from 105 to 21 s. The decrease in the % TN<sub>Conv.</sub> by the increase in the [C<sub>7</sub>H<sub>8</sub>]<sub>in</sub> is

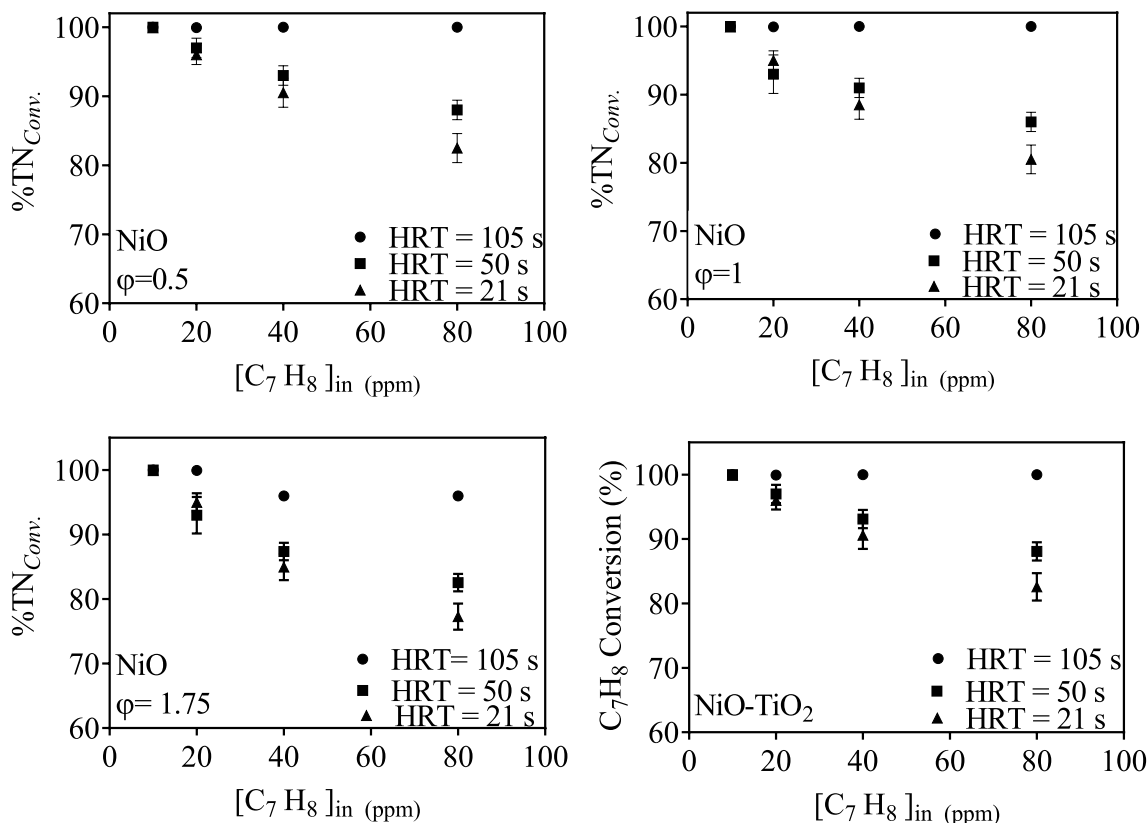


**Fig. 5** The effect of [C<sub>7</sub>H<sub>8</sub>]<sub>in</sub> on the % TN<sub>Conv.</sub> of toluene. Conditions: flow rate=0.1 to 0.5 L min<sup>-1</sup>, RH=10% and gas composition: [C<sub>7</sub>H<sub>8</sub>]<sub>in</sub>=40 ppm, 20% O<sub>2</sub> and the balance He

attributable to low residence time (i.e. short reaction time), which impacts the amount of toluene oxidized to CO<sub>2</sub> and other products. The oxidation of toluene occurs in two steps, beginning with the chemisorption of oxygen on the nano-catalysts, followed by the reaction of oxygen with toluene in the gas stream to produce CO<sub>2</sub>, water, and other products. As the HRT decreases (i.e. low reaction time) and the [C<sub>7</sub>H<sub>8</sub>]<sub>in</sub> increases, the chemisorption of oxygen conversely decreases and the % TN<sub>Conv.</sub> decreased.

### Effect of Relative Humidity (%RH)

Figure 6 presents the effect of %RH on toluene decomposition. Increasing the water content of the gas stream affected the % TN<sub>Conv.</sub>. The general trends showed that the %TN<sub>Conv.</sub> of toluene is significant when the %RH ≤ 20. However, higher %RH resulted in a noticeable decrease in conversion efficiency. Lower humidity enhanced the formation of hydroxyl radicals (·OH) from the dissociative chemisorption of water vapor [72–74] and increase the % TN<sub>Conv.</sub> at higher humidity, water will be adsorbed on the active site of the catalyst blocking the adsorption of VOCs and lowering the % TN<sub>Conv.</sub> [75, 76]. This may be attributed to the excessive water vapor on the surface of the catalyst, which

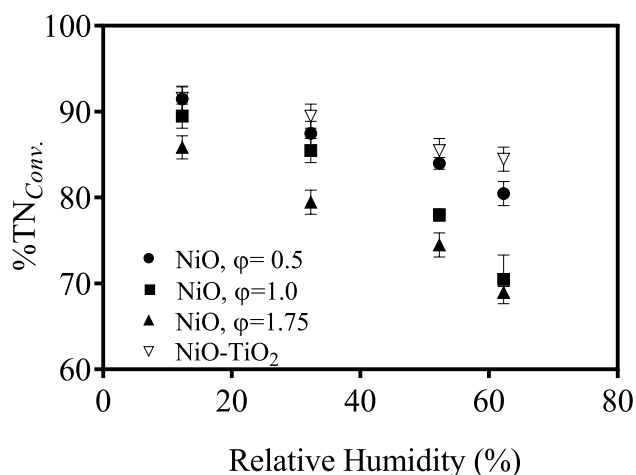


**Fig. 6** Effect of the %RH on the % TN<sub>Conv.</sub>. Conditions: HRT=50 s, flow rate=0.2 L min<sup>-1</sup> and gas composition: [C<sub>7</sub>H<sub>8</sub>]<sub>in</sub>=40 ppm, 20% O<sub>2</sub> and the balance He

**Table 2** Kinetic parameters of the studied nano-catalysts

Nano-catalysts	TOF (s <sup>-1</sup> ) × 10 <sup>-3</sup>		r (mol s <sup>-1</sup> g <sub>nano-powder</sub> )			E <sub>a</sub> (kJ mol <sup>-1</sup> )
	T = 100 °C	T = 140 °C	T = 100 °C	T = 140 °C	T = 160 °C	
Pure NiO	0.88	1.89	2.1	7.6	45	110
Mixed Ni–NiO	0.65	1.04	1.1	3.2	23	155
Pure Ni	0.55	0.95	0.78	1.9	11	180
NiO–TiO <sub>2</sub>	0.92	1.96	4.3	9.9	49	95

inhibits toluene oxidation due to the competition between the toluene and water for adsorption on the nano-catalysts active sites resulting in a decrease in the oxidation rate in what is called ‘competitive adsorption’ [89, 90]. For experiments conducted with [C<sub>7</sub>H<sub>8</sub>]<sub>in</sub> of 40 ppm, HRT=50 s, flow rate=0.2 L min<sup>-1</sup>, the % TN<sub>Conv.</sub> decreased by 11.5%, 20.0%, 19.6%, and 7.5% as the RH increased from 10 to 60 for the pure NiO, the mixture of Ni–NiO, pure Ni, and NiO–TiO<sub>2</sub>, respectively.

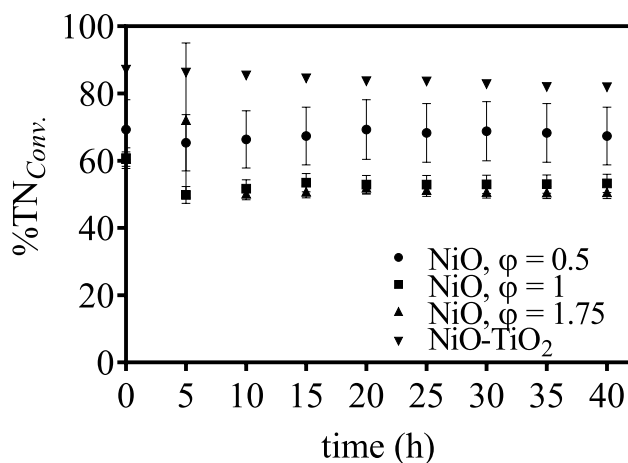
### Kinetic Parameters

Table 2 displays the toluene decomposition rate (*r*) normalized as a function of catalyst weight, and the catalyst turnover frequency (TOF) of the studied nano-catalysts. It was observed that pure NiO and NiO–TiO<sub>2</sub> had higher *r* and TOF compared to mixed Ni–NiO or pure Ni. This suggests a high reactivity for these nano-catalysts. The increase in *r* and TOF values for all of the nano-catalysts was proportional to temperature. The reaction rate of toluene decomposition per gram of catalyst. The catalytic reaction rate was the highest for NiO–TiO<sub>2</sub> followed by pure NiO. Lower *r* values were reported for a mixture of Ni–NiO and pure Ni. Previous studies regarding the catalytic oxidation of toluene to a proposed two-step oxidation mechanism: first, the oxygen chemisorption on the catalytic active site, and second, the surface reaction between toluene and adsorbed oxygen. Intermediates can also react with adsorbed oxygen. In this instance, the use of NiO and NiO–TiO<sub>2</sub> and the presence of oxygen in the structure of the nano-catalysts has eliminated the need for the first chemisorption step. Instead, toluene oxidation occurred once molecular toluene reached the surface of the catalyst. For mixed Ni–NiO and pure Ni, the catalyst must reach an excitation state, which causes the chemisorption oxygen to start the oxidation of toluene, which results in a lower reaction rate.

The activation energy for the conversion of toluene over NiO and NiO–TiO<sub>2</sub> nano-catalysts was calculated using Arrhenius Eq. (5):

$$r(\text{mol s}^{-1}) = A \exp\left(-\frac{E_a}{RT}\right) \quad (5)$$

where *E<sub>a</sub>* is the apparent activation energy (J mol<sup>-1</sup>), *R* is the universal gas constant (J mol<sup>-1</sup> K<sup>-1</sup>), *T* is the temperature



**Fig. 7** %  $TN_{Conv.}$  for extended process time (40 h). Experimental conditions: flow rate = 0.1 to 0.5 L  $min^{-1}$ , RH = 10% and gas composition:  $[C_7H_8]_{in} = 45$  ppm, 20%  $O_2$  and the balance He and  $T = 100$  °C

(K), and A is Arrhenius pre-exponential factor. A regression analysis of the experimental data by plotting  $\ln(r)$  versus  $1/T$  allows for the calculation of the activation energy for toluene oxidation (Table 2). Pure NiO and NiO–TiO<sub>2</sub> had lower  $E_a$  values within the range of 95–110 kJ  $mol^{-1}$  in comparison with high  $E_a$  for Ni–NiO and pure Ni nano-catalysts ( $\geq 155$  kJ  $mol^{-1}$ ). This indicates a lower energy requirement for the first two nanocatalysts is needed to achieve significant toluene oxidation.

### Stability Tests

Examining the stability of the catalysts was crucial in determining a practical application of this technology. Figure 7 illustrates the evolution of %  $TN_{Conv.}$  at 100 °C for 40 h. Pure NiO nano-catalysts exhibited a slight decrease in %  $TN_{Conv.}$  of toluene from 72 to 66% during the first five hours of operation, thereafter the %  $TN_{Conv.}$  of toluene was stabilized. However, Ni–NiO and pure Ni nano-catalysts showed a decrease in the %  $TN_{Conv.}$  in the range 11–15% and 17–22%, respectively, for the first eight hours of the reaction. After that period, the decrease in %  $TN_{Conv.}$  stabilized at approximately 12% and 17% lower than fresh nano-catalysts. However, after 15 h of operation, the %  $TN_{Conv.}$  increased, approaching 95% of the fresh catalyst conversion, and remained constant through to the end of the test. The decrease in %  $TN_{Conv.}$  during the preliminary oxidation time may be connected to the formation of coke [91], blocking of NiO active sites by water vapor, catalyst poisoning or fouling [92, 93]. Previous studies have shown that the deactivation of the catalyst by water vapor is reversible [94–96]. Based on the observed trends, it may be concluded that the cause for catalyst deactivation in the earliest stage is related to

blocking of NiO active sites by water vapor, which was present during the initial five hours of the test, and subsequently decreased after 8 hours. It is noteworthy that the NiO–TiO<sub>2</sub> nano-catalysts showed a stable oxidation capacity during the entirety of the test, which suggests that the deactivation factor on the catalyst was of limited effect.

### Toluene Decomposition Intermediates

FTIR measurements were conducted on the outlet gas to determine the possible intermediates of toluene decomposition. At low %  $TN_{Conv.}$  the FTIR spectra had four major peaks in the range of 1433 to 1600  $cm^{-1}$ , peaks in the range of 1383 to 1400  $cm^{-1}$ , and small peaks in the range of 3000 to 3500  $cm^{-1}$ . These peaks were assigned to the aromatic ring on the toluene, C–H bond in methyl group and non-identified hydrocarbon, respectively. However, when the reaction continued and the %  $TN_{Conv.}$  increased to 100%, the FTIR spectra displayed peaks at 3500 and 2400  $cm^{-1}$  which were assigned to benzene and CO<sub>2</sub>. The FTIR results indicate that the aromatic structure from toluene can be maintained for some time under the studied reaction condition. In contrast, as the time progressed with increases in system reactivity, the ring broke up into smaller hydrocarbons, which were detected in the FTIR but not identified.

### Conclusion

Ni–NiO and NiO–TiO<sub>2</sub> nano-catalysts synthesized by SCSM exhibited high catalytic activity toward toluene oxidation. Nano-catalysts with pure NiO and NiO–TiO<sub>2</sub> completely oxidized toluene in the gas stream. Whereas, Ni mixed with NiO or pure Ni metal required a greater amount of time and a higher temperature to achieve total toluene removal. Based on XPS, TEM, and FTIR data, pairing NiO with TiO<sub>2</sub> produced a nano-catalysts with a structure that enhanced the decomposition of toluene at low temperatures. NiO and NiO–TiO<sub>2</sub> demonstrated fast kinetic regimes in comparison with Ni mixed with NiO or pure Ni. The stability test showed synthesized nano-catalysts which exhibited a strong toluene conversion during a 40-h test.

**Acknowledgements** The authors acknowledge the financial support from Qatar University, International Research Collaboration Co-funds (IRCC-2020-011). The statements made herein are solely the responsibility of the authors.

**Funding** Open Access funding provided by the Qatar National Library.

**Open Access** This article is licensed under a Creative Commons Attribution 4.0 International License, which permits use, sharing,

adaptation, distribution and reproduction in any medium or format, as long as you give appropriate credit to the original author(s) and the source, provide a link to the Creative Commons licence, and indicate if changes were made. The images or other third party material in this article are included in the article's Creative Commons licence, unless indicated otherwise in a credit line to the material. If material is not included in the article's Creative Commons licence and your intended use is not permitted by statutory regulation or exceeds the permitted use, you will need to obtain permission directly from the copyright holder. To view a copy of this licence, visit <http://creativecommons.org/licenses/by/4.0/>.

## References

- Li, W.B., Wang, J.X., Gong, H.: Catalytic combustion of VOCs on non-noble metal catalysts. *Catal. Today* **148**(1), 81–87 (2009). <https://doi.org/10.1016/j.cattod.2009.03.007>
- Chlala, D., Labaki, M., Giraudon, J.-M., Gardoll, O., Denicourt-Nowicki, A., Roucoux, A., Lamonier, J.-F.: Toluene total oxidation over Pd and Au nanoparticles supported on hydroxyapatite. *C. R. Chim.* **19**(4), 525–537 (2016). <https://doi.org/10.1016/j.crci.2015.07.015>
- Beauchet, R., Magnoux, P., Mijoin, J.: Catalytic oxidation of volatile organic compounds (VOCs) mixture (isopropanol/o-xylene) on zeolite catalysts. *Catal. Today* **124**(3), 118–123 (2007). <https://doi.org/10.1016/j.cattod.2007.03.030>
- Kasperczyk, D., Urbaniec, K., Barbusinski, K., Rene, E.R., Colmenares-Quintero, R.F.: Application of a compact trickle-bed bioreactor for the removal of odor and volatile organic compounds emitted from a wastewater treatment plant. *J. Environ. Manag.* **236**, 413–419 (2019). <https://doi.org/10.1016/j.jenvman.2019.01.106>
- Zhong, L., Su, F.-C., Batterman, S.: Volatile Organic Compounds (VOCs) in conventional and high performance school buildings in the U.S. *Int. J. Environ. Res. Publ. Health* **14**(1), 100 (2017). <https://doi.org/10.3390/ijerph14010100>
- Chen, W.-H., Chen, Z.-B., Yuan, C.-S., Hung, C.-H., Ning, S.-K.: Investigating the differences between receptor and dispersion modeling for concentration prediction and health risk assessment of volatile organic compounds from petrochemical industrial complexes. *J. Environ. Manag.* **166**, 440–449 (2016). <https://doi.org/10.1016/j.jenvman.2015.10.050>
- Momani, F.A.: Treatment of air containing volatile organic carbon: elimination and post treatment. *Environ. Eng. Sci.* **24**(8), 1038–1047 (2007). <https://doi.org/10.1089/ees.2006.0162>
- Bravo, D., Ferrero, P., Peña-roja, J.M., Álvarez-Hornos, F.J., Gabaldón, C.: Control of VOCs from printing press air emissions by anaerobic bioscrubber: performance and microbial community of an on-site pilot unit. *J. Environ. Manag.* **197**, 287–295 (2017). <https://doi.org/10.1016/j.jenvman.2017.03.093>
- Hein, L., White, L., Miles, A., Roberts, P.: Analysing the impacts of air quality policies on ecosystem services; a case study for Telemark, Norway. *J. Environ. Manag.* **206**, 650–663 (2018). <https://doi.org/10.1016/j.jenvman.2017.10.073>
- Abdel-Raouf, M.E.-S., Abdel-Raheim, A.R.M., El-Saeed, S.M.: Thermo-catalytic versus thermo-chemical recycling of polystyrene waste. *Waste Biomass Valor.* **4**(1), 37–46 (2013)
- Dole, H.A.E., Isaifan, R.J., Sapountzi, F.M., Lizarraga, L., Aubert, D., Princivalle, A., Vernoux, P., Baranova, E.A.: Low temperature toluene oxidation over Pt nanoparticles supported on Ytria stabilized-zirconia. *Catal. Lett.* **143**(10), 996–1002 (2013). <https://doi.org/10.1007/s10562-013-1071-x>
- Momani, F.A., Jarrah, N.: Solar/UV-induced photocatalytic degradation of volatile toluene. *Environ. Technol.* **30**(10), 1085–1093 (2009). <https://doi.org/10.1080/09593330903079213>
- Pang, Y., Bosch, H., Hammer, T., Müller, D., Karl, J.: Plasma-aided reforming of toluene and isopropanol with analysis of decomposition mechanism. *Waste Biomass Valor.* **11**(2), 675–688 (2020)
- Labeau, O., Tamarat, P., Lounis, B.: Temperature dependence of the luminescence lifetime of single CdSe/ZnS quantum dots. *Phys. Rev. Lett.* **90**(25), 257404 (2003)
- Derwent, R., Jenkin, M., Saunders, S.: Photochemical ozone creation potentials for a large number of reactive hydrocarbons under European conditions. *Atmos. Environ.* **30**(2), 181–199 (1996)
- Zheng, J., Shao, M., Che, W., Zhang, L., Zhong, L., Zhang, Y., Streets, D.: Speciated VOC emission inventory and spatial patterns of ozone formation potential in the Pearl River Delta, China. *Environ. Sci. Technol.* **43**(22), 8580–8586 (2009)
- Jenck, J.F., Agterberg, F., Droescher, M.J.: Products and processes for a sustainable chemical industry: a review of achievements and prospects. *Green Chem.* **6**(11), 544–556 (2004)
- Kamal, A., Malik, R.N., Fatima, N., Rashid, A.: Chemical exposure in occupational settings and related health risks: a neglected area of research in Pakistan. *Environ. Toxicol. Pharmacol.* **34**(1), 46–58 (2012)
- Yu, Y., Hou, J., Li, M., Meng, F., Xi, B., Liu, D., Ye, M.: Selection and optimization of composting packing media for biofiltration of mixed waste odors. *Waste Biomass Valor.* **11**, 1–9 (2019)
- Leson, G., Winer, A.M.: Biofiltration: an innovative air pollution control technology for VOC emissions. *J. Air Waste Manag. Assoc.* **41**(8), 1045–1054 (1991)
- Oda, T.: Non-thermal plasma processing for environmental protection: decomposition of dilute VOCs in air. *J. Electrostat.* **57**(3–4), 293–311 (2003)
- Wani, A.H., Branion, R.M., Lau, A.K.: Biofiltration: a promising and cost-effective control technology for Odors, VOCs and air toxics. *J. Environ. Sci. Health Part A* **32**(7), 2027–2055 (1997)
- Preis, S., Klauson, D., Gregor, A.: Potential of electric discharge plasma methods in abatement of volatile organic compounds originating from the food industry. *J. Environ. Manag.* **114**, 125–138 (2013). <https://doi.org/10.1016/j.jenvman.2012.10.042>
- Mahmoodlu, M.G., Hassanizadeh, S.M., Hartog, N., Raouf, A., van Genuchten, M.T.: Evaluation of a horizontal permeable reactive barrier for preventing upward diffusion of volatile organic compounds through the unsaturated zone. *J. Environ. Manag.* **163**, 204–213 (2015). <https://doi.org/10.1016/j.jenvman.2015.08.025>
- Gruchlik, Y., Linge, K., Joll, C.: Removal of organic micropollutants in waste stabilisation ponds: a review. *J. Environ. Manag.* **206**, 202–214 (2018). <https://doi.org/10.1016/j.jenvman.2017.10.020>
- Chan, F.L., Keith, J.M.: Designing reverse-flow packed bed reactors for stable treatment of volatile organic compounds. *J. Environ. Manag.* **78**(3), 223–231 (2006). <https://doi.org/10.1016/j.jenvman.2005.04.019>
- Wu, H., Yan, H., Quan, Y., Zhao, H., Jiang, N., Yin, C.: Recent progress and perspectives in biotrickling filters for VOCs and odoriferous gases treatment. *J. Environ. Manag.* **222**, 409–419 (2018). <https://doi.org/10.1016/j.jenvman.2018.06.001>
- Hofstetter, T.B., Capello, C., Hungerbühler, K.: Environmentally preferable treatment options for industrial waste solvent management: a case study of a toluene containing waste solvent. *Process Saf. Environ. Prot.* **81**(3), 189–202 (2003). <https://doi.org/10.1205/095758203765639898>
- Gong, S., Liu, L., Zhang, J., Cui, Q.: Stable and eco-friendly solid acids as alternative to sulfuric acid in the liquid phase nitration of toluene. *Process Saf. Environ. Prot.* **92**(6), 577–582 (2014). <https://doi.org/10.1016/j.psep.2013.03.005>

30. Singh, R.S., Rai, B.N., Upadhyay, S.N.: Removal of toluene vapour from air stream using a biofilter packed with polyurethane foam. *Process Saf. Environ. Prot.* **88**(5), 366–371 (2010). <https://doi.org/10.1016/j.psep.2010.06.001>
31. Feng, Y., Wang, W., Wang, Y., Sun, J., Zhang, C., Mao, Y., Zhao, X., Song, Z.: Experimental study on in-situ decomposition of VOCs using microwave-induced metal discharge. *Waste Biomass Valor.* **10**(12), 3921–3929 (2019)
32. Chaturvedi, S., Dave, P.N., Shah, N.K.: Applications of nanocatalyst in new era. *J. Saudi Chem. Soc.* **16**(3), 307–325 (2012). <https://doi.org/10.1016/j.jscs.2011.01.015>
33. Bagheri, S., Muhd Julkapli, N., Bee Abd Ham id, S.: Titanium dioxide as a catalyst support in heterogeneous catalysis. *Sci. World J.* **2014**, 727496 (2014). <https://doi.org/10.1155/2014/727496>
34. Jiang, C., Jia, J., Zhai, S.: Mechanistic understanding of toxicity from nanocatalysts. *Int. J. Mol. Sci.* **15**(8), 13967–13992 (2014). <https://doi.org/10.3390/ijms150813967>
35. Bhosale, R.R., Kumar, A., Almomani, F., Alxneit, I.: Sol-gel derived CeO<sub>2</sub>-Fe<sub>2</sub>O<sub>3</sub> nanoparticles: synthesis, characterization and solar thermochemical application. *Ceram. Int.* **42**(6), 6728–6737 (2016). <https://doi.org/10.1016/j.ceramint.2016.01.042>
36. Khaki, M.R.D., Shafeeyan, M.S., Raman, A.A.A., Daud, W.M.A.W.: Application of doped photocatalysts for organic pollutant degradation—a review. *J. Environ. Manag.* **198**, 78–94 (2017). <https://doi.org/10.1016/j.jenvman.2017.04.099>
37. Liu, Y., Deng, J., Xie, S., Wang, Z., Dai, H.: Catalytic removal of volatile organic compounds using ordered porous transition metal oxide and supported noble metal catalysts. *Chin. J. Catal.* **37**(8), 1193–1205 (2016). [https://doi.org/10.1016/S1872-2067\(16\)62457-9](https://doi.org/10.1016/S1872-2067(16)62457-9)
38. Sinha, A.K., Suzuki, K.: Three-dimensional mesoporous chromium oxide: a highly efficient material for the elimination of volatile organic compounds. *Angew. Chem. Int. Ed.* **44**(2), 271–273 (2005)
39. Liotta, L.: Catalytic oxidation of volatile organic compounds on supported noble metals. *Appl. Catal. B* **100**(3–4), 403–412 (2010)
40. Alvarez-Galvan, M., De la Peña O’Shea, V., Fierro, J., Arias, P.: Alumina-supported manganese-and manganese–palladium oxide catalysts for VOCs combustion. *Catal. Commun.* **4**(5), 223–228 (2003)
41. Zhang, Z., Jiang, Z., Shangguan, W.: Low-temperature catalysis for VOCs removal in technology and application: a state-of-the-art review. *Catal. Today* **264**, 270–278 (2016)
42. Gonçalves, M., Guerreiro, M.C., de Oliveira, L.C.A., de Castro, C.S.: A friendly environmental material: Iron oxide dispersed over activated carbon from coffee husk for organic pollutants removal. *J. Environ. Manag.* **127**, 206–211 (2013). <https://doi.org/10.1016/j.jenvman.2013.05.017>
43. Ferrandon, M., Björnbom, E.: Hydrothermal stabilization by lanthanum of mixed metal oxides and noble metal catalysts for volatile organic compound removal. *J. Catal.* **200**(1), 148–159 (2001)
44. Barakat, T., Rooke, J.C., Tidahy, H.L., Hosseini, M., Cousin, R., Lamonier, J.F., Giraudon, J.M., De Weireld, G., Su, B.L., Siffert, S.: Noble-metal-based catalysts supported on zeolites and macroporous metal oxide supports for the total oxidation of volatile organic compounds. *ChemSuschem* **4**(10), 1420–1430 (2011)
45. Bhosale, R., Kumar, A., Almomani, F., Gupta, R.B.: Solar thermochemical ZnO/ZnSO<sub>4</sub> water splitting cycle for hydrogen production. *Int. J. Hydrog. Energy* **42**(37), 23474–23483 (2017). <https://doi.org/10.1016/j.ijhydene.2017.02.190>
46. Barakat, T., Rooke, J.C., Genty, E., Cousin, R., Siffert, S., Su, B.-L.: Gold catalysts in environmental remediation and water-gas shift technologies. *Energy Environ. Sci.* **6**(2), 371–391 (2013)
47. Jones, J.M., Dupont, V.A., Brydson, R., Fullerton, D.J., Nasri, N.S., Ross, A.B., Westwood, A.V.K.: Sulphur poisoning and regeneration of precious metal catalysed methane combustion. *Catal. Today* **81**(4), 589–601 (2003). [https://doi.org/10.1016/S0920-5861\(03\)00157-3](https://doi.org/10.1016/S0920-5861(03)00157-3)
48. Ahmadi, M., Haghighi, M., Kahforoushan, D.: Influence of active phase composition (Mn, Ni, Mn<sub>x</sub>Ni<sub>10-x</sub>) on catalytic properties and performance of clinoptilolite supported nanocatalysts synthesized using ultrasound energy toward abatement of toluene from polluted air. *Process Saf. Environ. Prot.* **106**, 294–308 (2017). <https://doi.org/10.1016/j.psep.2016.06.029>
49. Vu, V.H., Belkouch, J., Ould-Driss, A., Taouk, B.: Removal of hazardous chlorinated VOCs over Mn–Cu mixed oxide based catalyst. *J. Hazard. Mater.* **169**(1), 758–765 (2009). <https://doi.org/10.1016/j.jhazmat.2009.04.010>
50. Yao, X., Tang, C., Gao, F., Dong, L.: Research progress on the catalytic elimination of atmospheric molecular contaminants over supported metal-oxide catalysts. *Catal. Sci. Technol.* **4**(9), 2814–2829 (2014)
51. Azalim, S., Brahmi, R., Agunaou, M., Beaurain, A., Giraudon, J.M., Lamonier, J.F.: Washcoating of cordierite honeycomb with Ce–Zr–Mn mixed oxides for VOC catalytic oxidation. *Chem. Eng. J.* **223**, 536–546 (2013). <https://doi.org/10.1016/j.cej.2013.03.017>
52. Delannoy, L., Fajerweg, K., Lakshmanan, P., Potvin, C., Méthivier, C., Louis, C.: Supported gold catalysts for the decomposition of VOC: total oxidation of propene in low concentration as model reaction. *Appl. Catal. B* **94**(1), 117–124 (2010). <https://doi.org/10.1016/j.apcatb.2009.10.028>
53. Tang, C., Li, J., Yao, X., Sun, J., Cao, Y., Zhang, L., Gao, F., Deng, Y., Dong, L.: Mesoporous NiO–CeO<sub>2</sub> catalysts for CO oxidation: nickel content effect and mechanism aspect. *Appl. Catal. A* **494**, 77–86 (2015). <https://doi.org/10.1016/j.apcata.2015.01.037>
54. Bai, G., Dai, H., Deng, J., Liu, Y., Ji, K.: Porous NiO nanoflowers and nanourchins: Highly active catalysts for toluene combustion. *Catal. Commun.* **27**, 148–153 (2012). <https://doi.org/10.1016/j.catcom.2012.07.008>
55. Simeone, M., Salemme, L., Scognamiglio, D., Allouis, C., Volpicelli, G.: Effect of water addition and stoichiometry variations on temperature profiles in an autothermal methane reforming reactor with Ni catalyst. *Int. J. Hydrog. Energy* **33**(4), 1252–1261 (2008). <https://doi.org/10.1016/j.ijhydene.2007.12.034>
56. Gonzalez-Delacruz, V.M., Pereñiguez, R., Ternero, F., Holgado, J.P., Caballero, A.: Modifying the size of nickel metallic particles by H<sub>2</sub>/CO treatment in Ni/ZrO<sub>2</sub> methane dry reforming catalysts. *ACS Catal.* **1**(2), 82–88 (2011). <https://doi.org/10.1021/cs100116m>
57. Dardor, D., Bhosale, R., Kumar, A., Almomani, F.A., Gharbia, S., Ali, M.H., Folady, J., Yousefi, S., Jilani, M.: Computational thermodynamic analysis of solar fuel production via metal oxide based H<sub>2</sub>O and CO<sub>2</sub> splitting thermochemical cycles. In: *Emerging Technologies in Clean Energy for the 21st Century 2015 - Topical Conference at the 2015 AIChE Spring Meeting and 11th Global Congress on Process Safety 2015*, pp. 72–83
58. Shaban, M., Abukhadra, M.R., Hamd, A., Amin, R.R., Abdel Khalek, A.: Photocatalytic removal of Congo red dye using MCM-48/Ni<sub>2</sub>O<sub>3</sub> composite synthesized based on silica gel extracted from rice husk ash; fabrication and application. *J. Environ. Manag.* **204**, 189–199 (2017). <https://doi.org/10.1016/j.jenvman.2017.08.048>
59. Wang, D., Xu, R., Wang, X., Li, Y.: NiO nanorings and their unexpected catalytic property for CO oxidation. *Nanotechnology* **17**(4), 979 (2006)
60. Peng, G., Merte, L.R., Knudsen, J., Vang, R.T., Lægsgaard, E., Besenbacher, F., Mavrikakis, M.: On the mechanism of low-temperature CO oxidation on Ni (111) and NiO (111) surfaces. *J. Phys. Chem. C* **114**(49), 21579–21584 (2010)
61. Ackermann, M., Pedersen, T., Hendriksen, B., Robach, O., Bobaru, S., Popa, I., Quiros, C., Kim, H., Hammer, B., Ferrer, S.:

- Structure and reactivity of surface oxides on Pt (110) during catalytic CO oxidation. *Phys. Rev. Lett.* **95**(25), 255505 (2005)
62. Bhosale, R.R., Kumar, A., AlMomani, F., Ghosh, U., Sutar, P., Takalkar, G., Ashok, A., Alxneit, I.: Effectiveness of Ni incorporation in iron oxide crystal structure towards thermochemical CO<sub>2</sub> splitting reaction. *Ceram. Int.* **43**(6), 5150–5155 (2017)
  63. Wu, H., Wang, L., Zhang, J., Shen, Z., Zhao, J.: Catalytic oxidation of benzene, toluene and p-xylene over colloidal gold supported on zinc oxide catalyst. *Catal. Commun.* **12**(10), 859–865 (2011)
  64. Seo, H.O., Nam, J.W., Kim, K.-D., Sim, J.K., Kim, Y.D., Lim, D.C.: CO oxidation of Ni films supported by carbon fiber. *J. Mol. Catal. A* **361**, 45–51 (2012)
  65. Solsona, B., Garcia, T., Aylón, E., Dejoz, A.M., Vázquez, I., Agouram, S., Davies, T.E., Taylor, S.H.: Promoting the activity and selectivity of high surface area Ni–Ce–O mixed oxides by gold deposition for VOC catalytic combustion. *Chem. Eng. J.* **175**, 271–278 (2011)
  66. Kumar, A., Ashok, A., Bhosale, R.R., Saleh, M.A.H., Almomani, F.A., Al-Marri, M., Khader, M.M., Tarlochan, F.: In situ DRIFTS studies on Cu, Ni and CuNi catalysts for ethanol decomposition reaction. *Catal. Lett.* **146**(4), 778–787 (2016)
  67. Sharifi, M., Haghighi, M., Abdollahifar, M.: Hydrogen production via reforming of biogas over nanostructured Ni/Y catalyst: Effect of ultrasound irradiation and Ni-content on catalyst properties and performance. *Mater. Res. Bull.* **60**, 328–340 (2014). <https://doi.org/10.1016/j.materresbull.2014.07.027>
  68. Einaga, H., Futamura, S.: Effect of water vapor on catalytic oxidation of benzene with ozone on alumina-supported manganese oxides. *J. Catal.* **243**(2), 446–450 (2006)
  69. Zabihi, M., Shayegan, J., Fahimirad, M., Khorasheh, F.: Preparation, characterization and kinetic behavior of supported copper oxide catalysts on almond shell-based activated carbon for oxidation of toluene in air. *J. Porous Mater.* **22**(1), 101–118 (2015)
  70. Esmailirad, M., Zabihi, M., Shayegan, J., Khorasheh, F.: Oxidation of toluene in humid air by metal oxides supported on  $\gamma$ -alumina. *J. Hazard. Mater.* **333**, 293–307 (2017)
  71. Arnold III, E.W., Sundaresan, S.: Effect of water vapor on the activity and selectivity characteristics of a vanadium phosphate catalyst towards butane oxidation. *Appl. Catal.* **41**, 225–239 (1988)
  72. Zhang, S., Li, X.-S., Chen, B., Zhu, X., Shi, C., Zhu, A.-M.: CO oxidation activity at room temperature over Au/CeO<sub>2</sub> catalysts: disclosure of induction period and humidity effect. *ACS Catal.* **4**(10), 3481–3489 (2014)
  73. Huang, H., Ye, X., Huang, H., Zhang, L., Leung, D.Y.: Mechanistic study on formaldehyde removal over Pd/TiO<sub>2</sub> catalysts: Oxygen transfer and role of water vapor. *Chem. Eng. J.* **230**, 73–79 (2013)
  74. Chen, B.-B., Zhu, X.-B., Crocker, M., Wang, Y., Shi, C.: FeOx-supported gold catalysts for catalytic removal of formaldehyde at room temperature. *Appl. Catal. B* **154**, 73–81 (2014)
  75. Abdelouhab-Reddam, Z., Mail, R.E., Coloma, F., Sepúlveda-Escribano, A.: Platinum supported on highly-dispersed ceria on activated carbon for the total oxidation of VOCs. *Appl. Catal. A* **494**, 87–94 (2015). <https://doi.org/10.1016/j.apcata.2015.01.026>
  76. Xie, S., Dai, H., Deng, J., Yang, H., Han, W., Arandiyani, H., Guo, G.: Preparation and high catalytic performance of Au/3DOM Mn<sub>2</sub>O<sub>3</sub> for the oxidation of carbon monoxide and toluene. *J. Hazard. Mater.* **279**, 392–401 (2014). <https://doi.org/10.1016/j.jhazmat.2014.07.033>
  77. Guo, J., Xie, C., Lee, K., Guo, N., Miller, J.T., Janik, M.J., Song, C.: Improving the carbon resistance of Ni-based steam reforming catalyst by alloying with Rh: a computational study coupled with reforming experiments and EXAFS characterization. *ACS Catal.* **1**(6), 574–582 (2011)
  78. Kim, K.-D., Nam, J.W., Seo, H.O., Kim, Y.D., Lim, D.C.: Oxidation of toluene on bare and TiO<sub>2</sub>-covered NiO-Ni(OH)<sub>2</sub> nanoparticles. *J. Phys. Chem. C* **115**(46), 22954–22959 (2011). <https://doi.org/10.1021/jp2065997>
  79. Ashok, A., Kumar, A., Bhosale, R.R., Almomani, F., Saleh Saad, M.A.H., Suslov, S., Tarlochan, F.: Influence of fuel ratio on the performance of combustion synthesized bifunctional cobalt oxide catalysts for fuel cell application. *Int. J. Hydrog. Energy* (2018). <https://doi.org/10.1016/j.ijhydene.2018.02.111>
  80. Ashok, A., Kumar, A., Bhosale, R.R., Saleh, M.A.H., Ghosh, U.K., Al-Marri, M., Almomani, F.A., Khader, M.M., Tarlochan, F.: Cobalt oxide nanopowder synthesis using cellulose assisted combustion technique. *Ceram. Int.* **42**(11), 12771–12777 (2016). <https://doi.org/10.1016/j.ceramint.2016.05.035>
  81. MacKenzie, K.: The calcination of titania. IV. The effect of additives on the anatase-rutile transformation (1975).
  82. Gribb, A.A., Banfield, J.F.: Particle size effects on transformation kinetics and phase stability in nanocrystalline TiO<sub>2</sub>. *Am. Miner.* **82**(7–8), 717–728 (1997)
  83. Ahmed, M.: Synthesis and structural features of mesoporous NiO/TiO<sub>2</sub> nanocomposites prepared by sol–gel method for photodegradation of methylene blue dye. *J. Photochem. Photobiol. A* **238**, 63–70 (2012)
  84. Devi, L.G., Kottam, N., Murthy, B.N., Kumar, S.G.: Enhanced photocatalytic activity of transition metal ions Mn<sup>2+</sup>, Ni<sup>2+</sup> and Zn<sup>2+</sup> doped polycrystalline titania for the degradation of Aniline Blue under UV/solar light. *J. Mol. Catal. A* **328**(1–2), 44–52 (2010)
  85. Moulder, J.F., Stickle, W.F., Sobol, P.E., Bomben, K.D.: Handbook of X-ray photoelectron spectroscopy: a reference book of standard spectra for identification and interpretation of XPS data. Physical Electronics Division, Perkin-Elmer Corporation, 84–85 (1992).
  86. Park, E.J., Lee, J.H., Kim, K.-D., Kim, D.H., Jeong, M.-G., Kim, Y.D.: Toluene oxidation catalyzed by NiO/SiO<sub>2</sub> and NiO/TiO<sub>2</sub>/SiO<sub>2</sub>: Towards development of humidity-resistant catalysts. *Catal. Today* **260**, 100–106 (2016)
  87. Rooke, J.C., Barakat, T., Finol, M.F., Billemont, P., De Weireld, G., Li, Y., Cousin, R., Giraudon, J.M., Siffert, S., Lamonier, J.F., Su, B.L.: Influence of hierarchically porous niobium doped TiO<sub>2</sub> supports in the total catalytic oxidation of model VOCs over noble metal nanoparticles. *Appl. Catal. B* **142–143**, 149–160 (2013). <https://doi.org/10.1016/j.apcatb.2013.05.009>
  88. Kim, S.S., Park, K.H., Hong, S.C.: A study on HCHO oxidation characteristics at room temperature using a Pt/TiO<sub>2</sub> catalyst. *Appl. Catal. A* **398**(1), 96–103 (2011). <https://doi.org/10.1016/j.apcat.2011.03.018>
  89. Obee, T.N., Hay, S.O.: Effects of moisture and temperature on the photooxidation of ethylene on titania. *Environ. Sci. Technol.* **31**(7), 2034–2038 (1997). <https://doi.org/10.1021/es960827m>
  90. Pengyi, Z., Fuyan, L., Gang, Y., Qing, C., Wanpeng, Z.: A comparative study on decomposition of gaseous toluene by O<sub>3</sub>/UV, TiO<sub>2</sub>/UV and O<sub>3</sub>/TiO<sub>2</sub>/UV. *J. Photochem. Photobiol. A* **156**(1), 189–194 (2003). [https://doi.org/10.1016/S1010-6030\(02\)00432-X](https://doi.org/10.1016/S1010-6030(02)00432-X)
  91. Jacquemin, J., Siffert, S., Lamonier, J.F., Zhilinskaya, E., Aboukaïs, A.: Catalytic properties of beta zeolite exchanged with Pd and Fe for toluene total oxidation. In: Aiello, R., Giordano, G., Testa, F. (eds.) *Studies in Surface Science and Catalysis*, vol. 142, pp. 699–706. Elsevier (2002)
  92. Stasinska, B., Machocki, A., Antoniuk, K., Rotko, M., Figueiredo, J.L., Gonçalves, F.: Importance of palladium dispersion in Pd/Al<sub>2</sub>O<sub>3</sub> catalysts for complete oxidation of humid low-methane-air

- mixtures. *Catal. Today* **137**(2), 329–334 (2008). <https://doi.org/10.1016/j.cattod.2008.05.015>
93. Ojala, S., Lassi, U., Härkönen, M., Maunula, T., Silvonen, R., Keiski, R.L.: Durability of VOC catalysts in solvent emission oxidation. *Chem. Eng. J.* **120**(1), 11–16 (2006). <https://doi.org/10.1016/j.cej.2006.03.023>
94. Tan, W., Deng, J., Xie, S., Yang, H., Jiang, Y., Guo, G., Dai, H.: Ce<sub>0.6</sub>Zr<sub>0.3</sub>Y<sub>0.1</sub>O<sub>2</sub> nanorod supported gold and palladium alloy nanoparticles: high-performance catalysts for toluene oxidation. *Nanoscale* **7**(18), 8510–8523 (2015). <https://doi.org/10.1039/C5NR00614G>
95. Cordero-Lanzac, T., Aguayo, A.T., Gayubo, A.G., Castaño, P., Bilbao, J.: A comprehensive approach for designing different configurations of isothermal reactors with fast catalyst deactivation. *Chem. Eng. J.* **379**, 122260 (2020)
96. Flaherty, D.W., Yu, W.-Y., Pozun, Z.D., Henkelman, G., Mullins, C.B.: Mechanism for the water–gas shift reaction on monofunctional platinum and cause of catalyst deactivation. *J. Catal.* **282**(2), 278–288 (2011)

**Publisher's Note** Springer Nature remains neutral with regard to jurisdictional claims in published maps and institutional affiliations.